Article

Measuring Compositions in Organic Depth Profiling: Results from a VAMAS Interlaboratory Study

Alexander G. Shard,[*,†] Rasmus Havelund,[†] Steve J. Spencer,[†] Ian S. Gilmore,[†] Morgan R. Alexander,[‡] Tina B. Angerer,[§] Satoka Aoyagi,[∥] Jean-Paul Barnes,[⊥,#] Anass Benayad,[⊥,▽] Andrzej Bernasik,[○,1] Giacomo Ceccone,[◆,2] Jonathan D. P. Counsell,[¶] Christopher Deeks,[□,3] John S. Fletcher,[§] Daniel J. Graham,[⊗] Christian Heuser,[■] Tae Geol Lee,[▽,4] Camille Marie,[⊥,#] Mateusz M. Marzec,[○,5] Gautam Mishra,[●] Derk Rading,[±] Olivier Renault,[⊥,#] David J. Scurr,[‡] Hyun Kyong Shon,[▽] Valentina Spampinato,[▲] Hua Tian,[◇,6] Fuyi Wang,[★,7] Nicholas Winograd,[◇,6] Kui Wu,[★,7] Andreas Wucher,[■] Yufan Zhou,[$,8] and Zihua Zhu[$,8]

[†]National Physical Laboratory, Teddington, Middlesex TW11 0LW, United Kingdom
[‡]Laboratory of Biophysics and Surface Analysis, University of Nottingham, Nottingham NG7 2RD, United Kingdom
[§]Department of Chemistry and Molecular Biology, University of Gothenburg, Gothenburg 40530, Sweden
[∥]Department of Materials and Life Science, Seikei University, Tokyo 180-8633, Japan
[⊥]Université Grenoble Alpes, F-38000 Grenoble, France
[#]CEA, LETI, MINATEC Campus, F-38054 Grenoble, France
[▽]CEA-LITEN/DTNM, F-38054 Grenoble, France
[○]AGH University of Science and Technology, Al. Mickiewicza 30, 30-059 Kraków, Poland
[◆]Institute for Health and Consumer Protection, Via E. Fermi 2749, TP125, 21027 Ispra (VA), Italy
[¶]Kratos Analytical Ltd, Wharfside, Trafford Wharf Road, Manchester M17 1GP, United Kingdom
[□]Thermo Fisher Scientific, East Grinstead, West Sussex RH19 1UB, United Kingdom
[⊗]Department of Bioengineering, University of Washington, Seattle, Washington 98195, United States
[■]Faculty of Physics, University Duisburg-Essen, Lotharstraße 1, 47048 Duisburg, Germany
[▽]Korea Research Institute of Standards and Science, 267 Gajeong-ro, Yuseong-gu, Daejeon 305-340, Republic of Korea
[●]Corporate Research Analytical Laboratory (CRAL), 3M Deutschland GmbH, Carl-Schurz-Straße 1, Neuss 41460, Germany
[±]ION-TOF GmbH, Heisenberg Straße 15, D-48149 Münster, Germany
[▲]Istituto di Fisica dei Plasmi, Consiglio Nazionale delle Ricerche, Via R. Cozzi 53, 20125 Milano, Italy
[◇]Pennsylvania State University, 104 Chemistry Building, University Park, Pennsylvania 16802, United States
[★]CAS Key Laboratory of Analytical Chemistry for Living Biosystems, Chinese Academy of Sciences, Beijing 100190, China
[$]EMSL, Pacific Northwest National Laboratory, Richland, Washington 99354, United States

S *Supporting Information*

ABSTRACT: We report the results of a VAMAS (Versailles Project on Advanced Materials and Standards) interlaboratory study on the measurement of composition in organic depth profiling. Layered samples with known binary compositions of Irganox 1010 and either Irganox 1098 or Fmoc-pentafluoro-L-phenylalanine in each layer were manufactured in a single batch and distributed to more than 20 participating laboratories. The samples were analyzed using argon cluster ion sputtering and either X-ray photoelectron spectroscopy (XPS) or time-of-flight secondary ion mass spectrometry (ToF-SIMS) to generate depth profiles. Participants were asked to estimate the volume

continued...
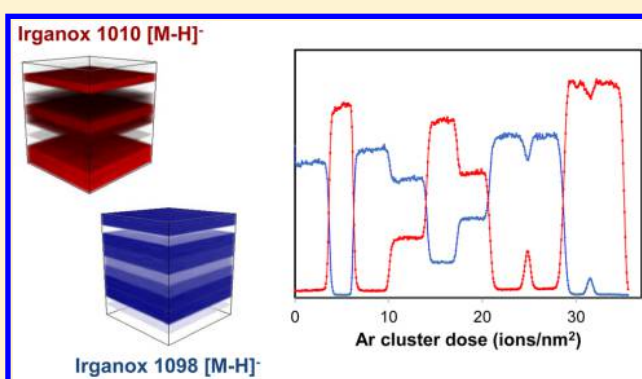
fractions in two of the layers and were provided with the compositions of all other layers. Participants using XPS provided volume fractions within 0.03 of the nominal values. Participants using ToF-SIMS either made no attempt, or used various methods that gave results ranging in error from 0.02 to over 0.10 in volume fraction, the latter representing a 50% relative error for a nominal volume fraction of 0.2. Error was predominantly caused by inadequacy in the ability to compensate for primary ion intensity variations and the matrix effect in SIMS. Matrix effects in these materials appear to be more pronounced as the number of atoms in both the primary analytical ion and the secondary ion increase. Using the participants' data we show that organic SIMS matrix effects can be measured and are remarkably consistent between instruments. We provide recommendations for identifying and compensating for matrix effects. Finally, we demonstrate, using a simple normalization method, that virtually all ToF-SIMS participants could have obtained estimates of volume fraction that were at least as accurate and consistent as XPS.

■ INTRODUCTION

There has been a profound advance in the analysis of organic and biological material through the use of gas cluster ion beams. Such clusters are capable of removing the surface layers of a sample by sputtering and exposing underlying material without imparting significant damage to the fresh surface. By using surface analytical techniques to measure the surface, either consecutively or simultaneously with sputtering, depth profiles and three-dimensional reconstructions of the chemistry of the sample can be obtained. This capability is of major importance in the development and understanding of techno-logical thin films, such as polymer blends,[1] solid state diffusion,[2] optical devices,[3] and organic light emitting diodes.[4] The approach has also found major use in the study of biological samples,[5] and is particularly useful for identifying the spatial distribution of small molecules, such as drugs and metabolites in single cells and tissue sections. Despite the fact that this technology is relatively new to many analysts, as commercial argon cluster sources for surface analytical equipment did not become available until 2010, more instruments are now sold with a gas cluster ion source than without one. Thus, there is a rapidly expanding community of analysts employing this method and a consequential requirement for fundamental understanding, valid methods, and useful data to support them.

The involvement of metrology institutes to assist these efforts has supported the rapid development and uptake of cluster ion beams for depth profiling. Early work at NIST identified the possibility of depth profiling organic materials using SF_5^+ clusters,[6] and subsequently, other types of cluster ions for sputtering organic materials were investigated.[7−9] However, identification of the best methods was not possible without adequate reference materials[10−13] which were both acceptable and accessible to researchers. Such materials are now available and have been employed to measure sputtering yields and depth resolutions to obtain underpinning data,[13−15] to develop descriptive models,[16,17] and to refine experimental methods.[18] Two VAMAS (Versailles Project on Advanced Materials and Standards) interlaboratory studies using vacuum evaporated layers of Irganox 1010 and Irganox 3114 clearly demonstrated the advantages of argon cluster sources for the depth profiling of organic materials.[19,20]

Currently there is a good understanding of the sputtering yield of a limited number of materials[21−23] and a growing understanding of the effects that contribute to depth resolution and the spatial reconstruction of chemistry from depth profiling data. However, the purpose of performing a depth profile or 3D reconstruction is usually to determine the concentration of particular species in different positions. This may be performed using a quantitative method, such as X-ray photoelectron spectroscopy (XPS), provided that care is taken to avoid effects such as X-ray,[24] electron beam,[25] and other forms[26] of damage

to delicate organic samples. Unfortunately, XPS is rather unspecific and cannot uniquely identify or distinguish different organic materials unless they contain distinctive elements or functional groups with clear chemical shifts in their core level binding energies. It is additionally rather insensitive, with detection limits[27] that restrict the applications for which it can be used. Time-of-flight secondary ion mass spectrometry (ToF-SIMS) offers the significant advantages of specificity and easier identification of molecular species. In the majority of situations it also provides better detection limits and spatial resolution than XPS.[28,29] However, the major weakness of ToF-SIMS is the lack of a clear and useful relationship between the intensity of secondary ions and the concentration of the material from which they arise. It is quite possible to observe no secondary ions from a material that is present in large concentrations in a mixture, even though they are observed from the pure material itself.[30] This is one of the well-known matrix effects in organic surface mass spectrometry,[31,32] which has defied any descrip-tion beyond phenomenology for many years. The most attractive approach to mitigate the matrix effect is to separate the ioniza-tion event from the sputtering process using, for example, laser post-ionization.[33,34] However, this is still in the early stages of development, and instruments are not widely available. There-fore, there is a need to identify, describe, and, if possible, compensate for matrix effects in a valid and practical manner to assist analysts in the conversion of ToF-SIMS data into useful measurements of composition.

One of the particular challenges in this endeavor is the pro-duction of reference materials with a known composition. Even if this can be accomplished, the effects of surface contamina-tion, damage, and segregation of components present an insurmountable challenge in terms of the stability and storage of such materials. In this respect, cluster ion sputtering offers an alternative approach. Through the creation of mixed materials as relatively thick films, it is possible to remove the unreliable surface material and access material at a depth where the composition is unaltered by surface effects. Such an approach has already been employed to identify the matrix effect and find preliminary descriptions of the behavior of mixed materials in ToF-SIMS experiments.[35,36] One of the critical and unanswered questions is whether a matrix effect which is found on a particular instrument and under certain operating conditions is the same as that found elsewhere. This becomes particularly important due to the increasing requirement to reproduce measurements, for example in the use of SIMS for measurement of intracellular drug concentration[37] to reduce attrition in drug development and improve drug efficiency,[38] and the expansion in choice of analytical ion beams, for example the growing use of argon clusters to obtain mass spectra with minimal fragmentation.[16]

This forms the motivation behind the interlaboratory study reported in this paper. The study was carried out under

the auspices of VAMAS Technical Working Area 2 (Surface Chemical Analysis) as subproject A3(g) "Static SIMS Interlaboratory Study: organic depth profiling of mixed materials". Two-component samples were distributed to participants: one sample, designated MMK, contained Irganox 1010 and Irganox 1098, and their mixture displays weak SIMS matrix effects under certain conditions. The other sample, designated MMF, comprising Irganox 1010 and Fmoc-pentafluoro-L-phenylalanine (FmocPFLPA), has strong SIMS matrix effects under the same conditions.[36] Each type of sample was created in a single batch so that, as far as possible, participants analyzed the same materials. Participants with the capability to perform XPS depth profiling were included, both to confirm the compositions of the mixed layers and to assess the capabilities and comparability of XPS for organic depth profiling. All participants possessed argon cluster sources; 15 participants returned at least one ToF-SIMS depth profile for each sample, and 6 participants returned at least one XPS depth profile for each sample. The participants were asked whether they could estimate the composition of two of the mixed layers using their data: 7 of the ToF-SIMS participants and 5 of the XPS participants attempted to do so. In this paper we comprehensively and consistently assess all the data returned to demonstrate unequivocally that matrix effects can be significant in ToF-SIMS depth profiles of organic materials. Furthermore, the magnitude and type of matrix effect is similar for most instruments and operating conditions, and the matrix effects for molecular secondary ions are more extreme and variable than those of lower mass secondary ions. XPS demonstrates much better consistency and accuracy in comparison to ToF-SIMS, although we note, in some data, that X-ray damage effects cannot be neglected, and may affect sputtering yields as suggested previously.[24]

■ EXPERIMENTAL SECTION

MMK and MMF samples were created by alternate evaporation of two materials in a custom-made QBox 450 (Mantis Deposition Ltd., Thame, U.K.) deposition unit equipped with independent evaporation cells, each with a shutter and a QCM to monitor the amount of material evaporated from the crucible. A schematic of this process has been provided previously.[19] The substrates for the samples comprised 10 mm square silicon wafers possessing ~20 nm layer of silicon oxide. There were 37 silicon wafers placed face down in a holder 24.5 cm above the crucibles. The substrate holder was rotated during deposition to improve coating uniformity across all samples. A shutter between the crucibles and substrate holder was opened and closed to start and finish each deposition step. The crucible heaters and shutters were controlled automatically using a computer with software provided by Mantis Deposition Ltd. The relationship between the thickness monitored by each crucible QCM and the thickness of material deposited on the silicon substrate was established prior to sample construction. A single evaporation of ~50 nm of material was monitored by the QCM; the precise thickness of the film was then measured by ellipsometry using an M2000DI spectroscopic ellipsometer (Woollam, NE). This formed the calibration step to translate QCM mass measurements into volume fractions for the mixed layers. The accuracy of ellipsometry for Irganox 1010 and FmocPFLPA films has previously been established through traceable X-ray reflectometry measurements and found to have a relative uncertainty of less than 4%.[39] The surface roughness of these types of samples is typically much less than 1 nm, as measured by AFM,[13] and ellipsometry modelling. X-ray

reflectometry[39] indicates that the interfacial roughness between materials is significantly smaller than the best depth resolution achievable by argon cluster depth profiling, ~5 nm.[20]

The structures of the MMK and MMF samples are provided schematically in Figure 1a. The batches of each material were formed using 309 individual evaporation steps, the numerical order of the layers shown in Figure 1a is the order they are encountered in a depth profile, which is the reverse order to the deposition sequence. The nominal thickness in layers 1−6 was 100 nm, and although there is some slight (at most 4%) variation from sample to sample depending upon their position in the sample holder, this is well-understood, proportionate for all layers, and does not affect any of the results reported here. Layer 2 is Irganox 1010, the structure of which is shown in Figure 1b. Layers 1 and 3 are FmocPFLPA, Figure 1c, in MMF samples and Irganox 1098, Figure 1d, in MMK samples; for brevity, in the following text and throughout we call these materials the analyte. Layers 4, 5, and 6 were each created through 50 pairs of sequential evaporations of Irganox 1010 and the analyte, each pair of steps producing a 2 nm increase in thickness. In layer 4, Irganox 1010 layers were 0.4 nm; in layer 5 Irganox 1010 layers were 1.6 nm, and in layer 6 Irganox 1010 layers were 1 nm thick. This generated mixed layers with volume fractions of Irganox 1010, ϕ_{1010}, were equal to 0.2, 0.8, and 0.5 (therefore analyte fractions 0.8, 0.2 and 0.5), respectively, for layers 4, 5, and 6. We had previously established that such a procedure generates films indistinguishable from mixed layers produced using submonolayer deposition steps[40] and, although time-consuming, is more controllable and reproducible than simultaneous coevaporation of two materials (data not shown). Layer 7 consists of a 3 nm layer of Irganox 1010 sandwiched between two 100 nm layers of analyte. Layer 8 consists of a 3 nm layer of analyte sandwiched between a 100 nm overlayer and a 150 nm underlayer of Irganox 1010. These thin marker layers are useful for assessing depth resolution, as described previously,[13] but were included here for a different purpose which will be described later.

Samples were dispatched to participants, along with a reference sample of Irganox 1010 of known thickness (~90 nm) so that participants could establish sputter rates prior to analyzing the MMK and MMF samples. A protocol[41] was also provided with general instructions on sample storage, handling, and data recording. The protocol provided guidance regarding analysis conditions and noted that detector saturation in SIMS and confirmation of a uniform sputtering dose in the analyzed area were items of particular concern. Previous investigations had shown that sample degradation occurs when this type of sample is exposed to temperatures of ~40 °C, and although participants were instructed to store the samples in a refrigerator, it is possible that samples sent outside the United Kingdom were exposed to such temperatures during transit. This appears to have been the case for one participant, who identified the issue and was supplied with new samples. However, it is possible that participant D also received damaged samples, and this may explain the poor depth resolution in their data.

Participants performed their analyses generally within six months of receiving the samples, and there was no evidence that prolonged periods of storage affected the data. Previous work at NPL has shown that the samples may be stored indefinitely (over one year) in refrigerated conditions: changes only occur for very thin (<10 nm) layers at the surface of the material, presumably due to slow segregation of components and accumulation of contaminants.
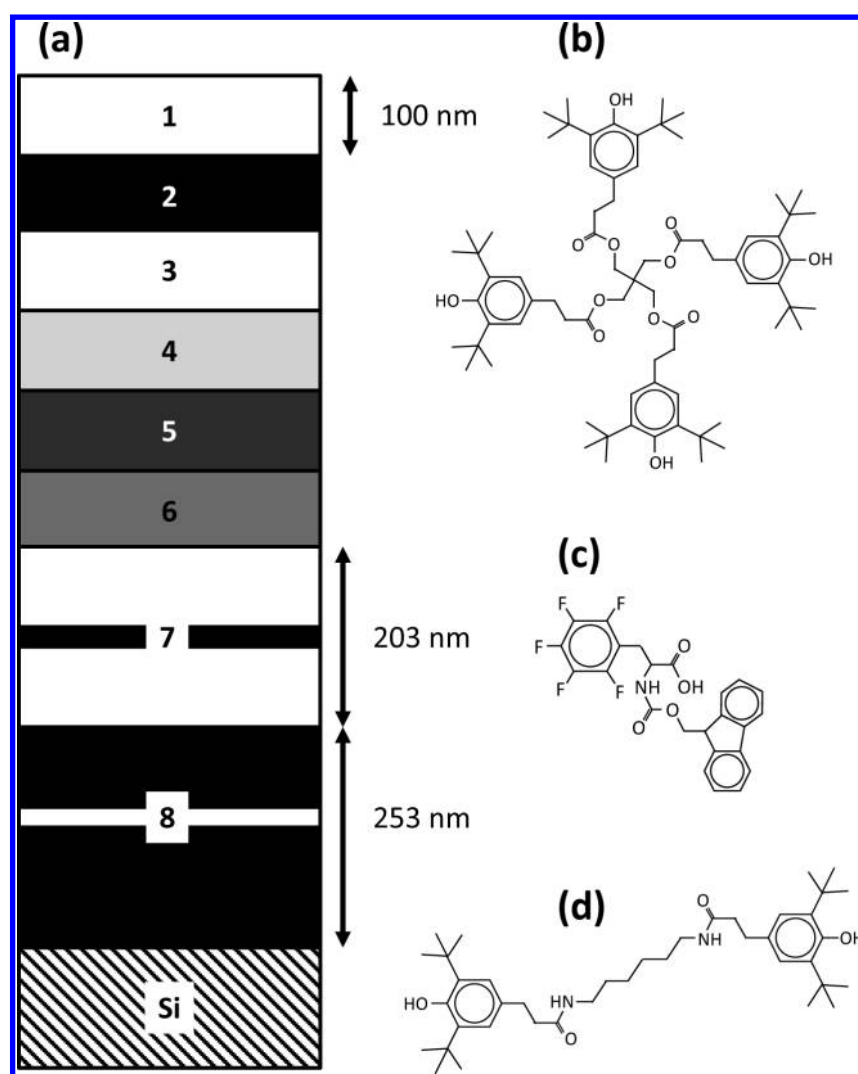
Figure 1. (a) Schematic of the structure of the multilayered samples used in this study. Samples are created by alternate evaporation of Irganox 1010 and either Irganox 1098 or Fmoc-PFLPA in MMK and MMF samples, respectively. Black indicates Irganox 1010, and white indicates the other component; mixed layers are indicated in grayscale. Thicknesses shown here are nominal, and the thicknesses of each organic layer on each sample are accurately known; see text for details. (b) The chemical structure of Irganox 1010. (c) The chemical structure of FmocPFLPA. (d) The chemical structure of Irganox 1098.

A summary of the equipment and conditions participants employed are provided in Table 1. Participants are designated by letters: A−O used ToF-SIMS instruments, while P−U used XPS instruments. Two laboratories returned both XPS and ToF-SIMS data but are identified as separate participants here. The argon cluster sources used for sputtering are indicated, as well as the analysis beam. Two participants (N and O) employed an instrument in which secondary ion analysis was performed upon the material ejected by the argon cluster sputtering process; a sequential sputter and analysis cycle was used by all other participants. All data returned was analyzed at NPL in a consistent manner, described later. All participants provided useful data that is included in this study. However, for a few participants, some of their sets of data were difficult or impossible to analyze and had to be excluded. Where this was the case, the reason is given in Table 1. Although depth resolution is not the subject of this study, we also record typical depth resolutions obtained by participants. In general the XPS data is too sparse to determine depth resolutions, and this was a result of participants following the guidance within the protocol

which specifically instructed participants to minimize X-ray exposure.

The participants were invited to attempt to quantify the volume fraction in layers 4 and 5 on the basis of the knowledge that layer 6 had a volume fraction $\phi_{1010} = 0.5$. The average discrepancies between the estimated values provided by participants and the nominal values are provided also in Table 1. The best methods for ToF-SIMS employed by participants G and J were to identify secondary ions that had close to half the intensity in layer 6 compared to the respective pure materials and use the intensities in layers 4 and 6 relative to the pure materials to calculate the compositions. This relies upon having a constant primary ion current.

We note here that a careful analysis of participants' data confirmed that Irganox 1010 and its mixtures with Fmoc-PFLPA had closely identical sputtering yields, although pure Fmoc-PFLPA has a slightly higher sputtering yield. Irganox 1098 was found to have a sputtering yield ~75% of Irganox 1010; however, these changes in yield do not influence the main findings of this paper and will be considered in detail elsewhere.

Table 1. List of Instruments, Sputtering Ion Sources, and Analysis Sources used by Participants in this Study[a]

| participant	type	instrument	Ar_n^+ energy	analysis source	notes	depth resolution	mean error in ϕ
A	SIMS	IONTOF TOF.SIMS 5	$n = 1000-2000$ 10−20 keV	Bi_3^+ 25 keV		18.5 nm	NA
B	SIMS	IONTOF TOF.SIMS 4	$n = 1000-2300$ 5−20 keV	Bi_3^+ 25 keV	strong intensity changes and detector saturation	21.3 nm	NA
C	SIMS	IONTOF TOF.SIMS 5−100	$n = 1500-4500$ 5−10 keV	Bi_5^+ 15 keV		13.0 nm	NA
D	SIMS	IONTOF TOF.SIMS 5	$n = 1700$ 10 keV	Bi_3^+ 30 keV	poor depth resolution (damaged samples?)		0.09 (MMF only)
E	SIMS	ULVAC PHI TRIFT V nanoTOF	$n = 2500$ 10 keV	Bi_3^+ 18 keV	detector saturation in one profile	21.8 nm	NA
F	SIMS	IONTOF TOF.SIMS 5	$n = 1600$ 10 keV	Bi_3^+ 15 keV and Ar_n^+ 10 keV		17.7 nm	NA
G	SIMS	IONTOF TOF.SIMS 5−100	$n = 1300$ 5 keV	Bi_3^+ 13 keV		14.8 nm	0.03 (MMK only)
H	SIMS	IONTOF TOF.SIMS 4	$n = 2000$ 5 keV	Bi^+, Bi_3^+, Bi_5^+ 25 keV	detector saturation in one profile	13.1 nm	0.06
I	SIMS	IONTOF TOF.SIMS 5	$n = 1500$ 20 keV	Bi_3^+ 25 keV	low secondary ion intensity for some ions	22.9 nm	NA
J	SIMS	IONTOF TOF.SIMS 5	$n = 1000$ 5−10 keV	Bi_3^{+2} 10 keV	strong intensity changes in a few profiles	18.1 nm	0.02
K	SIMS	IONTOF TOF.SIMS 4	$n = 600-1500$ 2.5 keV	Bi^+, Bi_3^+ 25 keV Bi_3^{+2} 50 keV	low secondary ion intensity for some ions	14.2 nm	NA
L	SIMS	IONTOF TOF.SIMS 5	$n = 1000$ 10 keV	Bi_3^+ 25 keV		15.0 nm	(0.11)
M	SIMS	IONTOF TOF.SIMS 5	$n = 1500-5000$ 10 keV	Bi_5^+ 30 keV		15.3 nm	(0.13)
N	SIMS	Ionoptika J105	$n = 1000-2000$ 10−20 keV	sputter beam	mass range limited, no data for some ions	13.9 nm	NA
O	SIMS	Ionoptika J105	$n = 4000$ (8% CO_2) 40 keV	sputter beam	mass range limited, no data for some ions	12.8 nm	0.07
P	XPS	ULVAC PHI Versaprobe II	$n = 2750$ 10 keV	Al Kα	poor depth resolution in some profiles		(0.04)
Q	XPS	Kratos AXIS Ultra DLD	$n = 2000$ 10 keV	Al Kα			0.01
R	XPS	Kratos AXIS Nova	$n = 1000-2000$ 5 keV	Al Kα	intensity variations in one profile		NA
S	XPS	ULVAC PHI Versaprobe II	$n = 1500$ 15 keV	Al Kα			(0.03)
T	XPS	Kratos AXIS Nova	$n = 1000-2000$ 5 keV	Al Kα		~13 nm	(0.03)
U	XPS	Thermo Fisher KAlpha+	$n = 2000$ 4 keV	Al Kα			(0.03)

[a]Challenges in the interpretation of data returned by participants are indicated in the notes column. Typical initial depth resolutions are also provided from each participant. Where participants returned estimates of composition, the mean error in ϕ from the nominal values is reported; NA denotes no attempt at quantification, and values in brackets denote that the calibration layer ($\phi = 0.50$) was not used in the participants method of composition estimation.

■ RESULTS AND DISCUSSION

XPS Depth Profiles. We turn first to the XPS data, which provides underpinning confirmation of the compositions of the materials. Figure 2a,b shows example profiles from the MMK and MMF samples, respectively, from data provided by participant T. Example profiles for other participants are provided in Supporting Information S1. The graphs show the atomic concentrations calculated in the normal manner by the participant using their own transmission function correction and sensitivity factors. The sputter time is converted into an approximate depth scale by scaling the time at which the substrate appears to the known thickness of the sample. This conversion assumes that sputtering yields are the same in both materials, which is not true for the MMK sample. The participants generally ignored the information provided regarding the composition of layer 6 and estimated the volume fractions of the mixed layers through the ratio of elemental compositions (specifically atom % nitrogen for MMK and atom % fluorine for MMF). The errors reported in Table 1 are, as expected, small and caused by either neglect to compensate for background intensity in the Irganox 1010 layers or neglect to compensate for X-ray degradation. In some cases it is clear that the sensitivity factors used by participants were not correct or not correctly applied, but this turns out not to be a significant source of error in the analysis we use here, see

Supporting Information S2. If, however, theoretical compositions were used to determine the mixed layer compositions, it would be a very significant source of error. Therefore, we recommend that, wherever possible, instrumental sensitivity factors are checked using pure compounds as part of routine spectrometer calibration.

The red line in Figure 2a,b is a fit to the data where each layer is represented by a box function convoluted with a Gaussian to represent the depth resolution at each interface; for layers 7 and 8, three layers are included. Five values of elemental composition were used: the two pure material compositions, X_1 (analyte) and X_0 (Irganox 1010), and compositions X_ϕ for layers 4, 5, and 6. The pure material compositions were assigned on the basis of the layer order, see Figure 1a. The width of each layer and full width half-maximum (fwhm) of the Gaussian are allowed to vary freely, with the exception of the marker layers in 7 and 8, which were set to 3 nm. Examination of Figure 2b demonstrates a slow drop in fluorine concentration for the pure material as the profile proceeds. This is almost certainly caused by X-ray degradation and is compensated by scaling the fitting function with an exponential decay. Without this correction, the MMF layer compositions are in error by an amount that depends upon which pure layer is used as the reference composition. The normalized intensity of the element
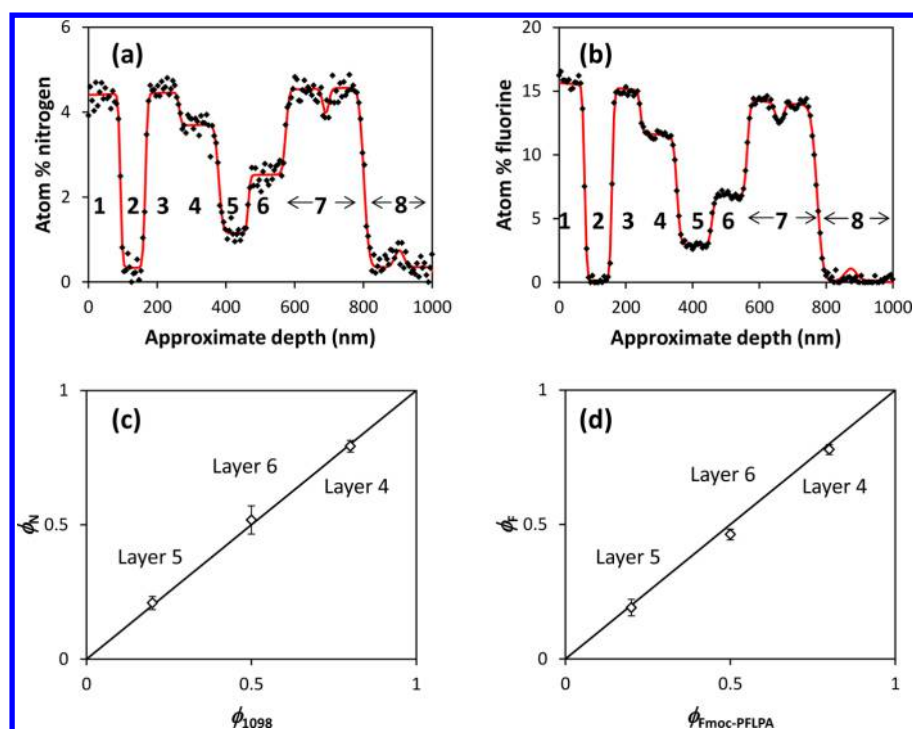
Figure 2. (a, b) Representative XPS depth profile data from (a) MMK and (b) MMF samples submitted by participant T. The sputtering source was 5 keV Ar_{1000}^+. Elemental compositions are shown as a function of dose, which has been converted into an approximate depth scale. The red continuous line is a description of the data using the model described in the text. Layers are identified by numbers using the system given in Figure 1. (c, d) XPS compositions for layers 4, 5, and 6 plotted against the nominal compositions. The mean for all useful data is shown for (c) MMK, 10 data sets, and (d) MMF samples, 12 data sets. The standard deviation of the data are shown as error bars.

ϕ_i, where i = N for MMK samples and i = F for MMF samples, provides an experimental measure of the composition:

$$\varphi_i = \frac{X_\varphi - X_0}{X_1 - X_0} \tag{1}$$

The mean of the resulting values and standard deviations as error bars are plotted as a function of the nominal compositions in Figure 2c,d. Here we find excellent agreement between the measured and nominal compositions, with some indication that the composition of MMF layer 6 is slightly less than $\phi_{\text{Fmoc-PFLPA}} = 0.5$, with the mean XPS value being $\phi_F = 0.47 \pm 0.02$. The scatter between participants for ϕ_N is somewhat larger than that for ϕ_F, and this is simply due to the much lower intensity of the N 1s signal for MMK samples compared to the F 1s signal for MMF samples, as is clear from the level of noise in Figure 2a,b.

ToF-SIMS Depth Profiles. Participants recorded specified secondary ion intensities as a function of the sputtering ion dose. The ions selected were based upon previous studies of similar materials[36] and were selected on the basis that they represented the pure materials (i.e., an intense signal from one material and virtually none from the other). Due to interferences, this necessitated a slightly different choice of secondary ions for Irganox 1010 in the MMK and MMF samples. A list of the secondary ions selected is provided in Table 2; in the remainder of the text, they are simply referred to by their nominal mass.

Figure 3 displays an example profile for an MMK sample from participant C, with all specified secondary ions shown. There is some variation in secondary ion intensity throughout the profile, particularly as the profile approaches the silicon interface. The variations in this data are not extreme and

Table 2. List of Secondary Ions Recorded by Participants

material	nominal mass (Da)	formula	accurate main isotopomer mass (Da)
Irganox 1010 (MMF)	41	C_2OH^-	41.003
Irganox 1010	59	$C_2O_2H_3^-$	59.013
Irganox 1010 (MMF)	231	$C_{16}OH_{23}^-$	231.175
Irganox 1010 (MMK)	277	$C_{17}O_3H_{25}^-$	277.180
Irganox 1010	1175	$C_{73}O_{12}H_{107}^-$ $(M - H)^-$	1175.776
Irganox 1098	26	CN^-	26.003
Irganox 1098	42	CNO^-	41.998
Irganox 1098	635	$C_{40}N_2O_4H_{63}^-$ $(M - H)^-$	635.479
Fmoc-PFLPA	19	F^-	18.998
Fmoc-PFLPA	167	$C_6F_5^-$	166.992
Fmoc-PFLPA	476	$C_{24}NO_4F_5H_{15}^-$ $(M - H)^-$	476.092
Fmoc-PFLPA	953	$C_{48}N_2O_8F_{10}H_{31}^-$ $(2M - H)^-$	953.192

insignificantly affect the most relevant data from layers 4, 5, and 6. Example profiles from other participants are provided in Supporting Information S1, where stronger variations are evident presumably due to primary beam instability. We retain the model used for the XPS data fitting, including the exponential term which compensates to some extent for smooth drifts in analytical ion beam intensity. The fit to each data set where it could be applied is shown as a red solid line. In data where the model was inadequate, average intensities were extracted from layers 2−6 for the purposes of later analysis. In about 5% of cases these layers could not be identified, and the data was discarded. The secondary ion at 277 Da demonstrates interesting background features in layers 1 and 7. The behavior
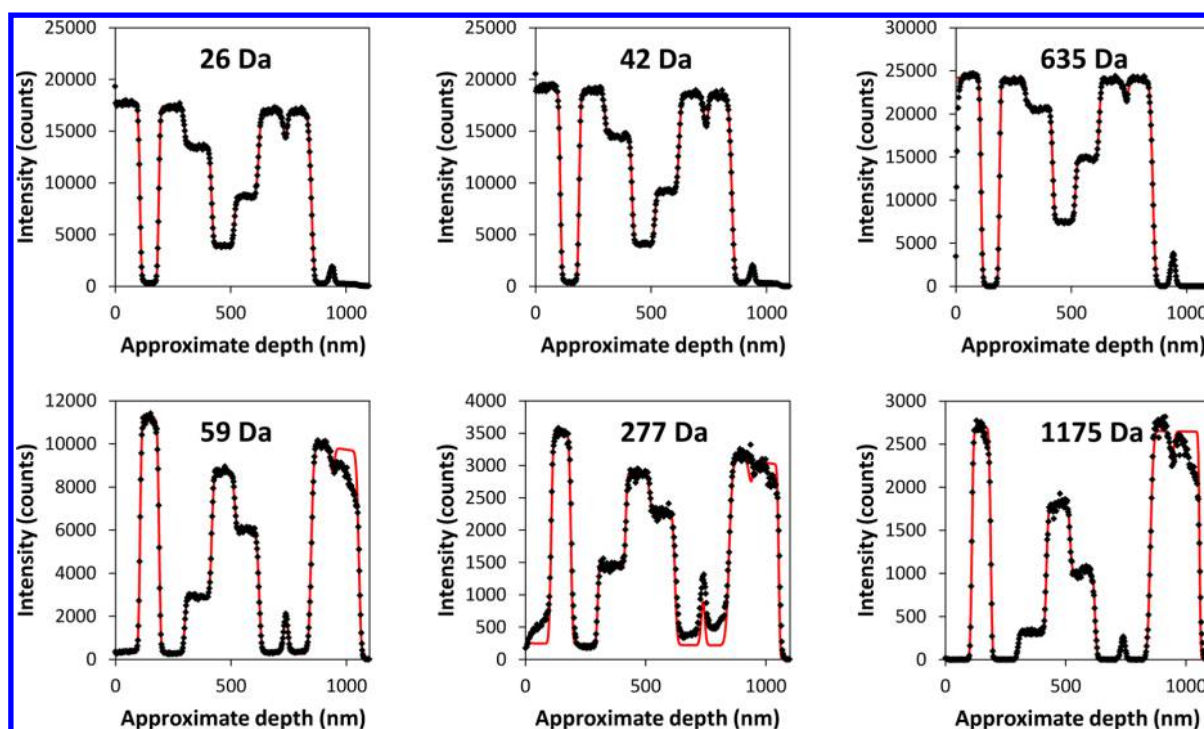
Figure 3. Representative SIMS depth profile data from an MMK sample submitted by participant C. The sputtering source was 5 keV Ar_{1500}^{+}, and the analysis source was 15 keV Bi_5^{+}. Six selected secondary ion intensities are shown as a function of dose, which has been converted into an approximate depth scale. The red continuous line is a description of the data using the model described in the text.
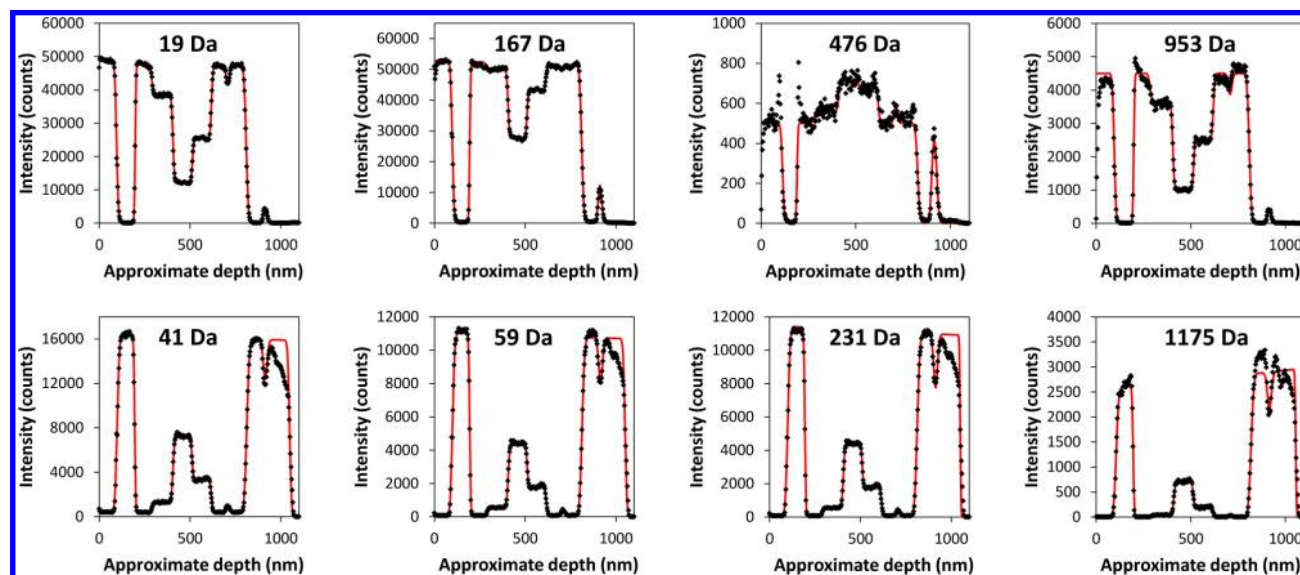

Figure 4. Representative SIMS depth profile data from an MMF sample submitted by participant C. The sputtering source was 5 keV Ar_{1500}^{+}, and the analysis source was 15 keV Bi_5^{+}. Eight selected secondary ion intensities are shown as a function of dose, which has been converted into an approximate depth scale. The red continuous line is a description of the data using the model described in the text.

of this profile strongly indicates that a contaminant in, or breakdown product of, Irganox 1010 is transferred to the vicinity of the Irganox 1098 crucible and then coevaporated with the Irganox 1098. It is only evident after prolonged Irganox 1010 evaporation, presumably because the Irganox 1098 crucible has to be cold for the condensation to occur. This would explain why there is no significant change in background in layer 3 since the Irganox 1098 crucible remains warm during the creation of the mixed layers. Participant O noted other secondary ions with a peculiar interfacial behavior, and although these were weak or absent in other participants' data, participant O had very different analysis conditions compared to most other participants which may enable a high sensitivity to certain molecular species. It is possible that such unknown species influence the secondary ion intensities investigated here; however, all indications are that such contaminants are in very small concentrations, and their presence does not change the general findings of this work.

Figure 4 displays a profile of the MMF sample from participant C. Here we note some interesting matrix effects, with
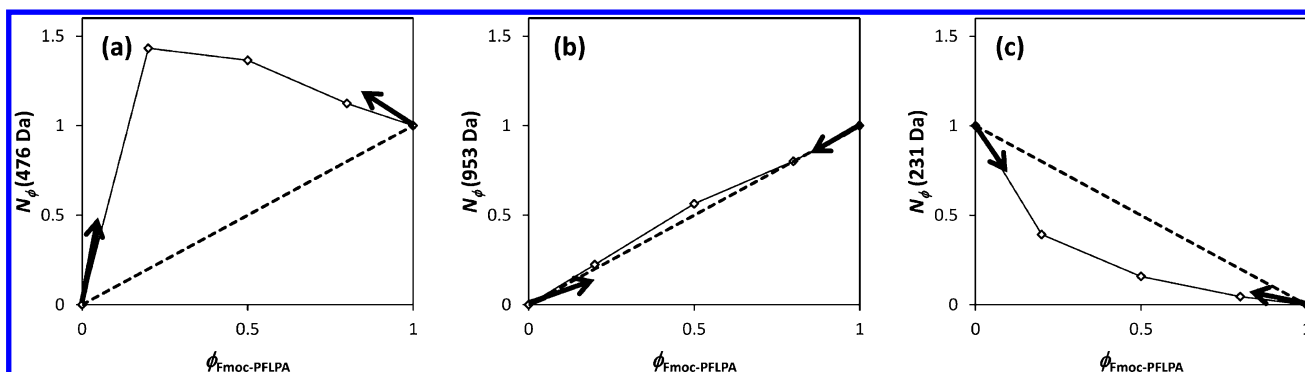
Figure 5. Normalized relative intensities, N_ϕ's, extracted from the data in Figure 4 for (a) 476 Da, (b) 953 Da, and (c) 231 Da secondary ions. Ideal behavior is shown as a dashed line, and the bold arrows indicate the gradients inferred from layers 7 and 8.

suppression of all secondary ions from Irganox 1010 in the mixed materials and enhancement of the Fmoc-PFLPA secondary ion at 167 Da, where there is little difference in intensity between $\phi_{\text{Fmoc-PFLPA}} = 1$ and $\phi_{\text{Fmoc-PFLPA}} = 0.8$, and extreme enhancement for the pseudomolecular secondary ion at 476 Da which has the highest secondary ion intensity in the most dilute mixture, $\phi_{\text{Fmoc-PFLPA}} = 0.2$. The spikes in intensity at the interfaces of layer 2 in this profile are perfectly explicable and a result of good depth resolution, we will consider these effects shortly. The deprotonated Fmoc-PFLPA dimer secondary ion at 953 Da exhibits some unexpected behavior in layers 3 and 7. In layer 3 the intensity declines throughout the layer, and in layer 7 there is a step change in intensity before and after the Irganox 1010 marker layer. These findings are confirmed by virtually all participants in the study, and the cause is unknown, but may relate to minor contaminants or the crystallinity of the material in these layers. For this reason, the secondary ion intensity in the pure material is somewhat uncertain and, because this is used as an intensity reference, means that the scatter in the data in the following analysis may be expected to be larger than for other secondary ions.

From our analysis of the profiles, we may extract for any secondary ion the mean intensity in each of the layers (corrected for gradual drift in analytical ion beam current by the exponential term), I_ϕ. By analogy to eq 1, we define a normalized relative intensity, N_ϕ, noting that in the absence of matrix effects this will be equivalent to the volume fraction, ϕ; we term the equivalence of N_ϕ and ϕ as "ideal" behavior.

$$N_\varphi = \frac{I_\varphi - I_0}{I_1 - I_0} \qquad (2)$$

In Figure 5 the values of N_ϕ are plotted against $\phi_{\text{Fmoc-PFLPA}}$ for three secondary ions from the profile shown in Figure 4 to demonstrate the three main behaviors: (a) enhancement, 476 Da; (b) close to ideal, 953 Da and; (c) suppression, 231 Da. To compare the magnitude of the enhancement and suppression, we follow a suggestion made previously[36] and quantify the matrix effect using the areas under the lines connecting the data points. We express this using an integral in eq 3, to indicate a formal definition, even though our evaluation of the area was as a discrete summation of polygons.

$$\Xi = 2 \int_0^1 N_\varphi \, d\varphi - 1 \qquad (3)$$

This provides the fractional difference in the area under the curve from the ideal case. Secondary ions which are enhanced

have positive values of Ξ, and those which are suppressed have negative values, for example: in Figure 5a, we obtain Ξ (476 Da) = +1.30; in Figure 5b, Ξ (953 Da) = +0.05; and in Figure 5c, Ξ (231 Da) = −0.49. This analysis provides a single metric through which we can compare the matrix effect found by participants in the study. We also examined the changes in intensity in the profile through the 3 nm markers in layers 7 and 8. Here, our analysis provided an apparent width for these layers, and the ratio of this to the known width should provide the limiting gradients for the plots in Figure 4 if the sputtering yields are identical in both materials and their mixtures. In the case of the marker in layer 7 for the 476 Da secondary ion, this was a negative width to fit the spike visible in Figure 4, and therefore a negative gradient close to $\phi_{\text{Fmoc-PFLPA}} = 1$. These limiting gradients are plotted in Figure 5 as bold arrows. Although they provide sensible results in most cases and are a simple way of determining matrix effects, we find that they are not precise enough to provide a comparator between participants.

Figure 6 displays the value of the matrix effect parameter, Ξ, for all data in the study that could be analyzed. The data are separated by sample and secondary ion: Figure 6a for MMK samples and Figure 6b for MMF samples. The average value of Ξ found for each secondary ion is plotted as a large dashed red circle; individual data are plotted as smaller symbols, and the symbol indicates the type of analytical primary ion employed by participants. We note first that, in general, there is excellent concordance between participants and, with the exception of the secondary ions at 167, 476, and 953 Da in MMF and the 635 Da secondary ion from MMK, the standard deviation in Ξ is less than 0.1, and often better than 0.05. No significant correlation was found between Ξ and the number of atoms in and energy of the Ar_n^+ ions used for sputtering, but some correlation was found with the identity of the analytical source. We have identified the results from participant F as solid red symbols because this participant employed an argon cluster analytical source for one set of profiles and a Bi_3^+ source in another using the same instrument. Therefore, when comparing these results, effects from the mass analyzer should be minimized and the major effects should be that of the primary ion used for analysis. The Bi_3^+ results for Ξ from this participant were indistinguishable from the average results.

Figure 6 demonstrates some clear trends from which conclusions can be drawn. First, atomic and low mass secondary ions demonstrate, consistently, the smallest magnitude of Ξ. Therefore, such species, providing that they are unique to the analyte, should be preferred for the purpose of reliable quantification in these materials. Second, secondary ions that are
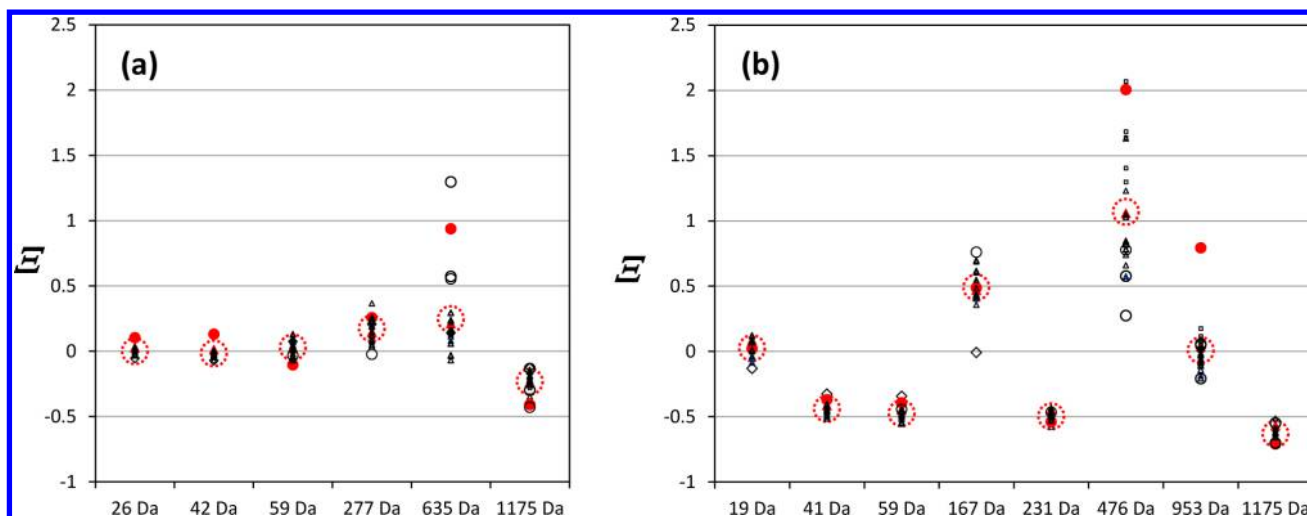
Figure 6. Magnitude and sign of the matrix effect parameter, Ξ, for selected ions and all useful data. The analytical beam is indicated by the following symbols: $\Diamond$, Bi^+; $\triangle$, Bi_3^+; $\square$, Bi_5^+; $\bigcirc$, Ar_n^+. The mean value is indicated by a dashed red circle. Data from participant F who employed both Bi_3^+ and Ar_n^+ on the same instrument are indicated by filled red symbols: (a) MMK samples, 25 data sets; (b) MMF samples, 24 data sets.

suppressed (i.e., have negative Ξ) have a more consistent matrix effect than those that are enhanced. This may be a particular effect of these sample systems, but if the result is general this should be taken into account when comparing data between instruments. Third, the primary ion chosen for the analytical beam can produce strong variations in matrix effect enhancements. For example, the 635 Da secondary ion in MMK samples is moderately enhanced using bismuth sources, but has a very strong enhancement (with Ξ of the order +1) using argon cluster sources. This result is echoed in the MMF samples, with the enhancement for the 476 Da secondary ion using Bi_5^+ clearly separable from the Bi_3^+ results. Here, the argon cluster results are less clear and much more scattered; notably, the result for participant F is at odds with those from participants N and O who used a different instrument design.

There are correlations between the measured values of Ξ for different secondary ions. We find excellent linear correlations between Ξ (26 Da) and Ξ (42 Da) in MMK ($R^2 = 0.94$) and Ξ (41 Da) and Ξ (59 Da) in MMF ($R^2 = 0.96$). Since these secondary ions originate from the same materials, this correlation is almost certainly a reflection of variations in primary ion current across the profiles which are inadequately compensated in our analysis. There is some evidence from the MMK samples that Ξ (635 Da) and Ξ (1175 Da) in MMK are anticorrelated ($R^2 = 0.64$), suggesting that the enhancement of the Irganox 1098 pseudomolecular ion and the suppression of the Irganox 1010 pseudomolecular ion are connected. However, this correlation relies largely upon the three laboratories using argon cluster sources. There are no other correlations of significance. These correlations, or lack thereof, are important because they strongly suggest that the most important source of scatter and variability between participants arises from analytical ion source instability and drift which could be eliminated by careful measurement, improved equipment design, or an adequate data normalization scheme.

Before proceeding to the consequences of the matrix effect in quantitative analysis, we note a relationship that may be useful in assessing its presence and magnitude. In Figure 7 we plot the normalized intensity of secondary ions at 50% volume fraction, $N_{0.5}$, against Ξ. Here, there is an excellent linear correspondence: the correlation is unsurprising since $N_{0.5}$ is a major contributor in
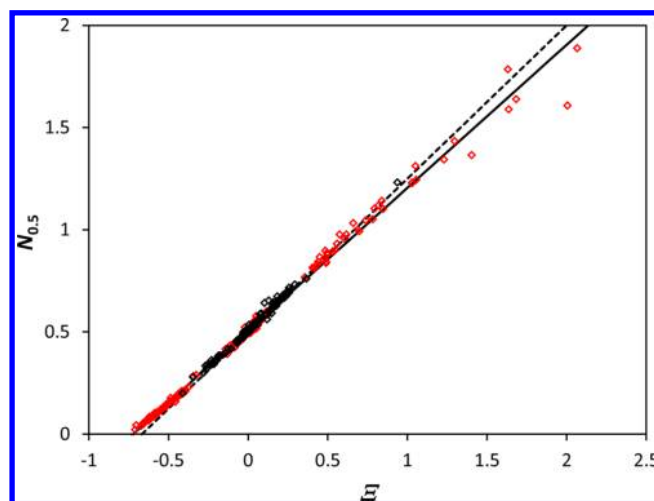
Figure 7. Normalized intensity at $\phi_{1010} = 0.5$, $N_{0.5}$, for secondary ions plotted as a function of the matrix effect parameter, Ξ, extracted from individual secondary ion profiles for all useful profiles (296 data points). Data from MMK samples are black, and data from MMF samples are red. The solid black line is a least-squares fit to the data, and the dashed line represents the expected relationship from Simpson's rule with gradient $^3/_4$.

the calculation of Ξ. With $\Xi = 0$ we expect $N_{0.5} = 0.5$, and linear regression through the data provides a slope of 0.7. Application of Simpson's rule, which assumes a quadratic form for the curve connecting N_0, $N_{0.5}$, and N_1, indicates that a slope of 0.75 should be expected, and this must be correct for very small matrix effects ($\Xi \rightarrow 0$). The quadratic form is clearly in error for large matrix effects, see Figure 5a, and the assessment of area using Simpson's rule must fail for strong suppression ($\Xi < -^2/_3$). However, it is encouraging to see that linearity appears to extend over a wide range, and therefore, the value of Ξ can be measured using only one mixture of known composition close to $\phi = 0.5$ and a quadratic form for N_ϕ, provided that Ξ is between approximately -0.5 and $+1$.

SIMS Matrix Effect in Thickness and Yield Measurements. Having established the presence of matrix effects in organic SIMS for all participants, and finding that in most cases there is no great variation between participants using the same
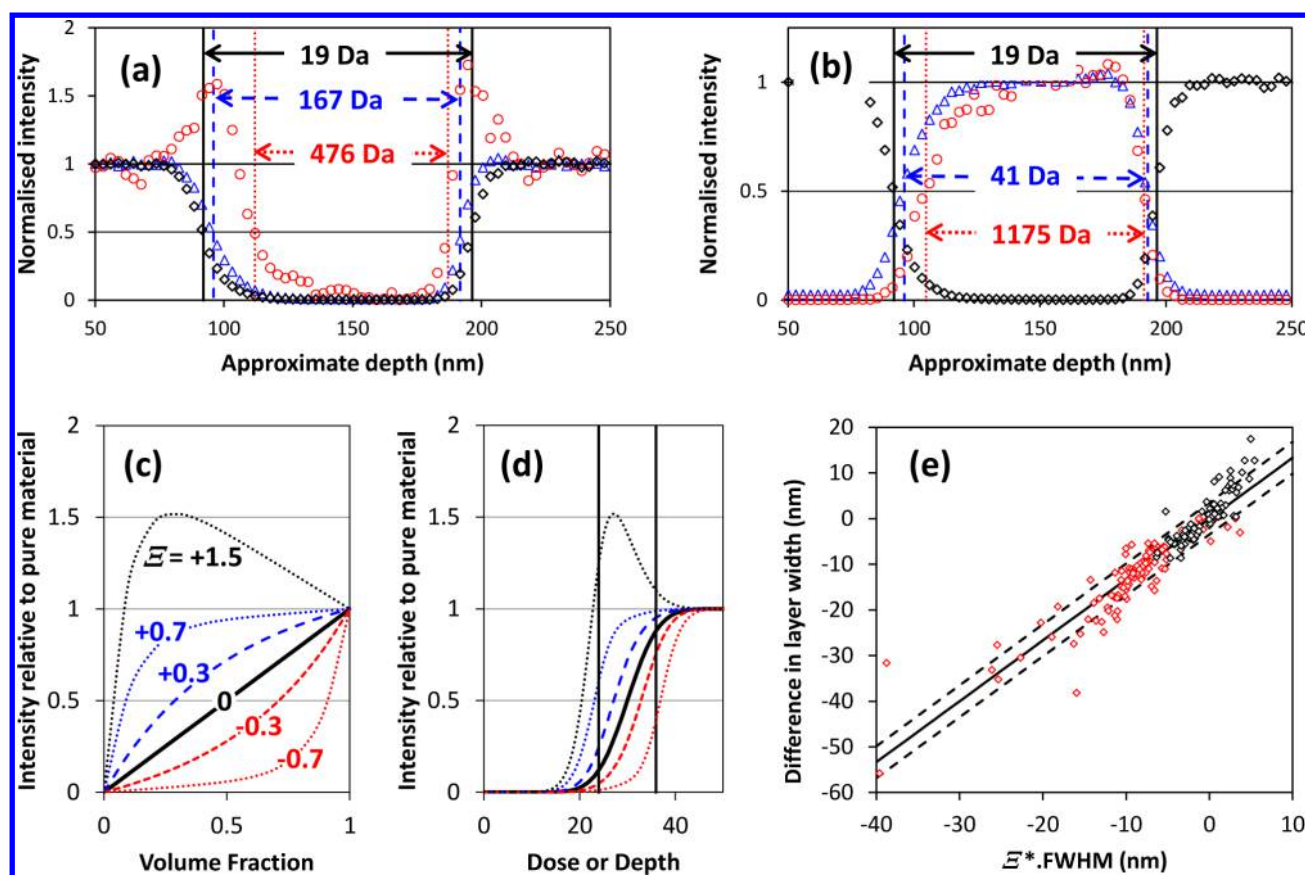
Figure 8. (a) Data from participant M, using 10 keV Ar_{3000}^+ and 30 keV Bi_5^+. Layer 2 in the profile is shown, with widths inferred from different 50% secondary ion intensities: ◇ black, 19 Da (reference width); △ blue, 167 Da (width difference, −8 nm); ◯, 476 Da (−28 nm). (b) Secondary ions from layer 2: △ blue, 41 Da (−7 nm); ◯, 1175 Da (−17 nm). (c) Example plots of N_ϕ with values of Ξ marked. (d) Predicted secondary ion intensities using the relationships in part c for a model interface, with fwhm resolution shown by vertical lines. (e) The difference in layer 2 width from the reference width (26 Da in MMK samples and 19 Da in MMF samples) plotted against the product of Ξ^* (modified Ξ, see text) and the mean fwhm for reference ions for all other secondary ions, extracted from individual secondary ion profiles for all useful profiles (225 data points). Data from MMK samples are black, and data from MMF samples are red. The black solid line has gradient $^4/_3$, and the dashed lines represent the root-mean-square scatter of the data about this line.

analytical ion source, we demonstrate the influence these effects have on depth profiling data and the manner in which they may be corrected. We turn first to the measurement of the position of an interface in a depth profile, which is important, for example, in measuring the thickness of an organic layer.

The established method of defining an interface in a SIMS depth profile is to determine the position at which the secondary ion intensity is half that of the pure material. This, of course, works if there are no matrix effects. In Figure 8a,b we display data from a single depth profile of participant M in the region of layer 2 of an MMF sample. In Figure 8a all of the secondary ions originate from layers 1 and 3, and each provides a different width. We have established that the 19 Da ion has no matrix effect, and therefore, this secondary ion provides our reference width. The other secondary ions are enhanced in the mixture, and both indicate that the layer width is smaller than the reference value. In Figure 8b we compare the 19 Da profile to secondary ions from layer 2 itself; all secondary ions from this material are suppressed, and these also provide a width smaller than the reference value. In this sample, virtually all secondary ions provide incorrect layer widths, and only through our knowledge of which secondary ions are free from matrix effects (or by using XPS data) can we establish the sputtering yields of Fmoc-PFLPA and Irganox 1010 and its mixtures.

In Figure 8c,d the origin of the effect is demonstrated: we apply the example N_ϕ relationships shown in Figure 8c to a step function convolved with a Gaussian given by the solid black line in Figure 8d. Since the 50% intensity does not correspond to the 50% composition, there is a shift in the apparent position of the interface, which may be larger than the half width at half-maximum of the Gaussian. The full width at half-maximum is shown by the vertical lines. Visual inspection of the data to identify this effect is not helpful unless $\Xi > +1$, when intensities greater than that in the pure material are found at the interface, as shown by the 476 Da ion in Figure 8a. If such effects are observed, it indicates that it will be virtually impossible to extract a meaningful interface position from the data. The purpose of Figure 8d is to illustrate that the interface position depends upon a convolution of the matrix effect with the depth resolution of the experiment. The depth scale in this figure is arbitrary, and the curves can be scaled simply by changing the fwhm of the interface. This assumes that the matrix effect has the same influence at all depth resolutions, which is probably not the case because at the interface a range of compositions are sampled,[36] but is a useful assumption in establishing the magnitude of the effect.

We demonstrate this effect using the participants' data in which we plot the difference in layer 2 width from a reference

value, taken from secondary ions without matrix effect, against the product of the fwhm depth resolution and a modified parameter Ξ. The fwhm is taken as the mean value at the two interfaces, and Ξ^* is $+\Xi$ if the secondary ion is from layer 2 and $-\Xi$ if it is from layers 1 and 3. Here we find reasonable linearity with proportionality constant $\sim^4/_3$ and a scatter of ~3.5 nm. The data with a positive change in layer width, which deviate from the line, arise from the 277 Da secondary ion in MMK samples which have unusual background features as noted previously and are therefore less reliable. Notably, the width of the layer may be in error by more than 10 nm without any large matrix effect, and this source of uncertainty should be considered in measurements of sputtering yield and layer thickness using ToF-SIMS. However, since the relationship appears well-behaved, it may also be used to estimate matrix effect magnitudes or conversely, with knowledge of them, correct layer thickness measurements.

**SIMS Matrix Effect in Composition Measurements.** Until this point, the comparison of SIMS and XPS data has been somewhat unfair. The XPS data has been normalized, using a well-established procedure, to eliminate source fluctuations whereas the SIMS data, for lack of any valid procedure, has been presented as raw intensities. In this section we demonstrate a SIMS normalization procedure that provides useful results and, had the participants had access to it prior to this study, would have enabled the vast majority to measure the two unknown compositions with very small error. It is also far more desirable to use high molecular weight secondary ions than small fragments because their relationship to the analyte is more certain. In this section we validate a simple procedure to use molecular, or at least high mass fragment, secondary ions to provide compositional information with excellent precision and note the limitations that matrix effects place upon the selection of such secondary ions.

The essential equation is given in eq 4. This relates the intensities of secondary ion A, unique to component a, and secondary ion B, unique to component b, to the composition of the mixture, expressed as volume fraction, ϕ_a, where it is assumed $\phi_a + \phi_b = 1$. Note that if the ions are not unique, then background intensities from the other component should be subtracted to provide the respective intensities I_A and I_B. The factor $k(A{:}B)$ is a relative sensitivity factor and is generally applicable over a narrow range of compositions and experimental conditions.

$$\varphi_a = I_A/(I_A + k(A{:}B)I_B) \tag{4}$$

In the general case, $k(A{:}B)$ is defined as the secondary ion intensity ratio I_A/I_B when $\phi_a = \phi_b$. This requires analysis of a 50:50 uniform mixture of the two components, and we term the relative sensitivity factor determined in this manner as k_{50} calculated as $I_A(\phi_a = 0.5)/I_B(\phi_b = 0.5)$. Alternatively, the ratio of secondary ion intensities from the pure materials may be used. We term the relative sensitivity factor determined in this manner as k_p calculated as $I_A(\phi_a = 1)/I_B(\phi_b = 1)$. If both ions behave in an ideal manner, then $k_p = k_{50}$. Otherwise, if the components are phase separated, k_p is preferred, and if they are mixed, k_{50} is preferred.

Figure 9 shows some example data from participants following the application of this method. In Figure 9a, data from participant J is displayed from the MMK sample. This set of data had little change in primary current throughout the profile, and the normalized 26 Da intensity reflects the composition of the sample with reasonable accuracy. Also plotted
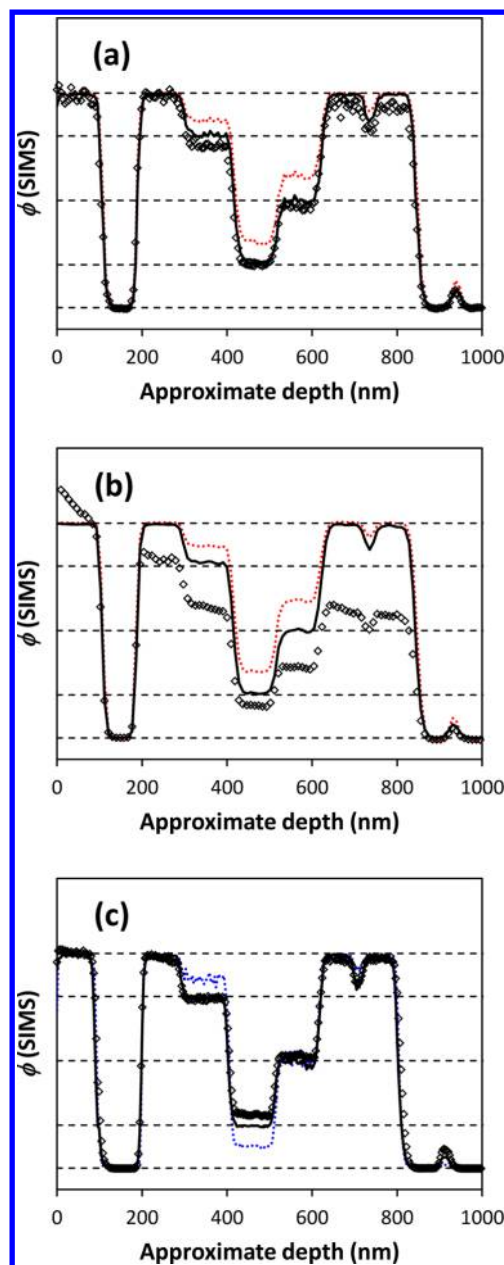
Figure 9. Normalization procedure for SIMS showing calculated volume fraction against approximate depth. Horizontal black dashed lines indicate nominal layer compositions: 0 (bottom), 0.2, 0.5, 0.8, and 1 (top). (a) MMK data from participant J: $\Diamond$ normalized 26 Da intensity, interpreted as ϕ; ϕ calculated using 635 and 1175 Da intensities with $k_p = 17.3$ (red, dashed line) and $k_{50} = 27.5$ (black, solid line). (b) As part a for participant L: $k_p = 17.3$ and $k_{50} = 31.0$. (c) MMF data from participant C: $\Diamond$ normalized 19 Da intensity; ϕ calculated using 953 and 1175 Da intensities with $k_{50} = 12.5$ (blue, dashed line) and using 167 and 59 Da intensities with $k_{50} = 26.0$ (black, solid line).

are the results of applying eq 4 to the pseudomolecular secondary ions at 635 Da $(M_{1098} - H)^-$, $\Xi \sim +0.25$, and 1175 Da $(M_{1010} - H)^-$, $\Xi \sim -0.23$. The red dashed line indicates results using $k_p = 17.3$, and the black solid line was obtained by setting layer 6 to the nominal composition using $k_{50} = 27.5$. Black horizontal dashed lines indicate the nominal compositions, and these are matched by the black solid line to within $\Delta\phi \sim 0.01$. Note that the slight drift in intensity observed for the 26 Da secondary ion is eliminated. We apply the same method to

a profile provided by participant L in Figure 9b where, as can be seen from the 26 Da intensity, strong variation in primary beam current was observed. After normalization using the same method using k_p = 17.3, and k_{50} = 31.0 (both derived from the data in the profile), we find nearly identical results to those of participant J. Across all the data that permits analysis, we find that the same secondary ions provide closely identical compositions from the participant's data: layer 5 ϕ_{1098}(SIMS) = 0.82 and layer 4 ϕ_{1098}(SIMS) = 0.22, with a standard deviation in ϕ of 0.02. The standard deviation drops to 0.01 after removing two clear outliers: participant K who had very weak intensity at 1185 Da and participant N who experienced intensity fluctuations throughout the profile.

The approach requires some caution; in Figure 9c we display data from participant C using eq 4 applied to the combination of the 953 Da $(2M_{Fmoc-PFLPA} - H)^-$, $\Xi \sim +0.01$, and 1175 Da $(M_{1010} - H)^-$, $\Xi \sim -0.63$, secondary ions as a blue dashed line. Here, one secondary ion displays a strong matrix effect, and the other has virtually none. The predicted compositions for layers 4 and 5 are in error by $\Delta\phi \sim 0.1$. However, the method applied to the fragments at 167 Da ($\Xi \sim +0.50$) and 59 Da ($\Xi \sim -0.47$) shown by the black line are much better, indicating that ions from one material that are enhanced should be paired with ions from the other that are suppressed. Using these results we can provide recommendations and limitations for the application of eq 4 in the analysis of binary mixtures: (1) Reference samples which include the pure materials and, as a minimum, one mixture of known composition close to $\phi = 0.5$ should be analyzed. (2) The matrix effect for characteristic secondary ions should be estimated from these data. (3) Secondary ions selected for quantitative analysis using eq 4 should be chosen such that Ξ_A, Ξ_B, and the sum $(\Xi_A + \Xi_B)$ are all as close to zero as possible.

When applying the method to a depth profile it should be noted that it will provide useful results if the composition is relatively uniform across the analyzed area. Particular care should be taken if there is a rapid change in composition, such as at material interfaces, for two reasons. First, a wide range of compositions will contribute to the data, and unless neither secondary ion has a matrix effect, neither k_p nor k_{50} will be useful. Second, the two secondary ions may provide information from different depths into the material,[20] and this may introduce significant distortion in the profile. Additionally, the range over which eq 4 remains valid is not yet clear; it may fail if the composition is far from the calibration point (i.e., in the dilute regimes in this case), yet with care, it appears useful over an impressive range of compositions ($\phi < 0.2$ to $\phi > 0.8$).

Summary and Outlook. This work represents a significant advance toward quantitative depth profiling of organic materials using both XPS and ToF-SIMS. We have demonstrated that, through the use of good reference materials, it is possible to provide insight and confidence in methods for the analysis of binary mixtures. The important finding of the study is that SIMS matrix effects are broadly similar in all types of instrument, and the major source of variation appears to be the analytical primary species. While not all the effects found in this study have been adequately explained, there are clear general findings: (1) Matrix effects are weaker in atomic, diatomic, and low mass secondary ions than they are for molecular species. (2) Matrix effects tend to be more severe as the number of atoms in the primary ion cluster increases. (3) A consistent normalization scheme can be found for ToF-SIMS data and applied to molecular secondary ions to obtain realistic and reproducible compositions.

Now that it is possible to measure the matrix effect in binary mixtures using the methods described in this paper, there remains the task of cataloguing and either understanding or describing them. We hope that, in the near future, it will be possible to predict the main types of matrix effect with reasonable certainty from the chemistry of the components, and this will reduce the requirement for reference materials. Since binary mixtures can be of great importance in technological materials, such as organic photovoltaics and light emitting diodes, this is an important step. However, there is another significant step to make in applying such rules to ternary or higher mixtures. It is a matter of great significance, for example in the measurement of biological materials, whether the methods that are appropriate for binary mixtures can be used to obtain the relative composition of two components in the presence of a third component.

CONCLUSIONS

This interlaboratory study has shown that compositional analysis in organic depth profiling is achievable. For XPS, it is a relatively straightforward matter, but we note that the effects of X-ray damage need to be considered for some of the samples we used here, and therefore for materials in general. Participants using ToF-SIMS provided data that, as we have shown, were capable of providing consistent and accurate compositions. However, since there is a lack of guidance or validated procedures in the literature, the majority were not able to analyze the data appropriately. Of those that were able to do so, the best method from participants G and J relied upon stability in the analytical ion current throughout the profile. Other participants would not be able to use such methods on their data due to drift in the analytical ion beam current during the profile.

We have used the participants' data to measure the matrix effect in ToF-SIMS for the selected secondary ions and find that the results are remarkably consistent; the scatter in the data appears largely due to analytical ion current variations that could not be adequately compensated. The major factors that influence matrix effects are the identity of the primary ion, argon clusters generally producing larger matrix effects than bismuth clusters, and the identity of the secondary ion, with low mass fragments generally having smaller matrix effects than molecular fragments and pseudomolecular species. The influence that the matrix effect has on measurements of physical quantities, such as the thickness of a buried organic layer and the composition of the layer, are considered in detail in this paper, and we provide recommendations for correcting data for these influences.

ASSOCIATED CONTENT

ⓢ Supporting Information

The Supporting Information is available free of charge on the ACS Publications website at DOI: 10.1021/acs.jpcb.5b05625.

> Example depth profiles from each participants on both material systems, XPS compositions of layers from relevant participants, and calculation of errors introduced through the use of incorrect XPS sensitivity factors (PDF)

AUTHOR INFORMATION

Corresponding Author
*E-mail: alex.shard@npl.co.uk.

Notes

The authors declare no competing financial interest.

[1]Complete affiliation address: Faculty of Physics and Applied Computer Science, AGH-University of Science and Technology, Al. Mickiewicza 30, 30-059 Kraków, Poland.

[2]Complete affiliation address: European Commission, Joint Research Centre, Institute for Health and Consumer Protection, Nanobiosciences Unit, Via E. Fermi 2749, TP125, 21027 Ispra (VA) Italy.

[3]Complete affiliation address: Thermo Fisher Scientific, Unit 24, The Birches Industrial Estate, Imberhorne Lane, East Grinstead, West Sussex RH19 1UB, United Kingdom.

[4]Complete affiliation address: Center for Nano-Bio Measurement, Korea Research Institute of Standards and Science, 267 Gajeong-ro, Yuseong-gu, Daejeon 305-340, Republic of Korea.

[5]Complete affiliation address: Academic Centre for Materials and Nanotechnology, AGH-University of Science and Technology, Al. Mickiewicza 30, 30-059 Kraków, Poland.

[6]Complete affiliation address: Department of Chemistry, Pennsylvania State University, 104 Chemistry Building, University Park, Pennsylvania 16802, United States.

[7]Complete affiliation address: CAS Key Laboratory of Analytical Chemistry for Living Biosystems, Institute of Chemistry, Chinese Academy of Sciences, Beijing 100190, China.

[8]Complete affiliation address: W. R. Wiley Environmental Molecular Sciences Laboratory, Pacific Northwest National Laboratory, Richland, Washington 99354, Unites States.

■ REFERENCES

(1) Terlier, T.; Tiron, R.; Gharbi, A.; Chevalier, X.; Veillerot, M.; Martinez, E.; Barnes, J. P. Investigation of block depth distribution in ps-b-pmma block copolymer using ultra-low-energy cesium sputtering in tof-sims. *Surf. Interface Anal.* **2014**, *46*, 83−91.

(2) Gilbert, J. B.; Rubner, M. F.; Cohen, R. E. Depth-profiling x-ray photoelectron spectroscopy (xps) analysis of interlayer diffusion in polyelectrolyte multilayers. *Proc. Natl. Acad. Sci. U. S. A.* **2013**, *110*, 6651−6656.

(3) Bailey, J.; Havelund, R.; Sharp, J. S.; Shard, A. G.; Gilmore, I. S.; Alexander, M. R.; Scurr, D. J. 3d tof-sims imaging of polymer multilayer films using argon cluster sputter depth profiling. *ACS Appl. Mater. Interfaces* **2015**, *7*, 2654−2659.

(4) Aizawa, N.; Pu, Y.-J.; Watanabe, M.; Chiba, T.; Ideta, K.; Toyota, N.; Igarashi, M.; Suzuri, Y.; Sasabe, H.; Kido, J. Solution-processed multilayer small-molecule light-emitting devices with high-efficiency white-light emission. *Nat. Commun.* **2014**, *5*, 5756.

(5) Fletcher, J. S. Latest applications of 3d tof-sims bio-imaging. *Biointerphases* **2015**, *10*, 018902.

(6) Gillen, G.; Roberson, S. Preliminary evaluation of an sf5+ polyatomic primary ion beam for analysis of organic thin films by secondary ion mass spectrometry. *Rapid Commun. Mass Spectrom.* **1998**, *12*, 1303−1312.

(7) Weibel, D.; Wong, S.; Lockyer, N.; Blenkinsopp, P.; Hill, R.; Vickerman, J. C. A C-60 primary ion beam system for time of flight secondary ion mass spectrometry: Its development and secondary ion yield characteristics. *Anal. Chem.* **2003**, *75*, 1754−1764.

(8) Ninomiya, S.; Ichiki, K.; Yamada, H.; Nakata, Y.; Seki, T.; Aoki, T.; Matsuo, J. Precise and fast secondary ion mass spectrometry depth profiling of polymer materials with large ar cluster ion beams. *Rapid Commun. Mass Spectrom.* **2009**, *23*, 1601−1606.

(9) Ninomiya, S.; Ichiki, K.; Yamada, H.; Nakata, Y.; Seki, T.; Aoki, T.; Matsuo, J. Molecular depth profiling of multilayer structures of organic semiconductor materials by secondary ion mass spectrometry with large argon cluster ion beams. *Rapid Commun. Mass Spectrom.* **2009**, *23*, 3264−3268.

(10) Shard, A. G.; Brewer, P. J.; Green, F. M.; Gilmore, I. S. Measurement of sputtering yields and damage in c60sims depth profiling of model organic materials. *Surf. Interface Anal.* **2007**, *39*, 294−298.

(11) Wagner, M. S. Molecular depth profiling of multilayer polymer films using time-of-flight secondary ion mass spectrometry. *Anal. Chem.* **2005**, *77*, 911−922.

(12) Lu, C. Y.; Wucher, A.; Winograd, N. Molecular depth profiling of buried lipid bilayers using C-60-secondary ion mass spectrometry. *Anal. Chem.* **2011**, *83*, 351−358.

(13) Shard, A. G.; Green, F. M.; Brewer, P. J.; Seah, M. P.; Gilmore, I. S. Quantitative molecular depth profiling of organic delta-layers by c-60 ion sputtering and sims. *J. Phys. Chem. B* **2008**, *112*, 2596−2605.

(14) Delcorte, A.; Garrison, B. J. Sputtering polymers with buckminsterfullerene projectiles: A coarse-grain molecular dynamics study. *J. Phys. Chem. C* **2007**, *111*, 15312−15324.

(15) Lee, J. L. S.; Ninomiya, S.; Matsuo, J.; Gilmore, I. S.; Seah, M. P.; Shard, A. G. Organic depth profiling of a nanostructured delta layer reference material using large argon cluster ions. *Anal. Chem.* **2010**, *82*, 98−105.

(16) Seah, M. P.; Havelund, R.; Gilmore, I. S. Universal equation for argon cluster size-dependence of secondary ion spectra in sims of organic materials. *J. Phys. Chem. C* **2014**, *118*, 12862−12872.

(17) Seah, M. P.; Spencer, S. J.; Shard, A. G. Angle-dependence of argon gas cluster sputtering yields for organic materials. *J. Phys. Chem. B* **2015**, *119*, 3297−3303.

(18) Sjovall, P.; Rading, D.; Ray, S.; Yang, L.; Shard, A. G. Sample cooling or rotation improves C-60 organic depth profiles of multilayered reference samples: Results from a vamas interlaboratory study. *J. Phys. Chem. B* **2010**, *114*, 769−774.

(19) Shard, A. G.; Ray, S.; Seah, M. P.; Yang, L. Vamas interlaboratory study on organic depth profiling. *Surf. Interface Anal.* **2011**, *43*, 1240−1250.

(20) Shard, A. G.; Havelund, R.; Seah, M. P.; Spencer, S. J.; Gilmore, I. S.; Winograd, N.; Mao, D.; Miyayama, T.; Niehuis, E.; Rading, D.; Moellers, R. Argon cluster ion beams for organic depth profiling: Results from a vamas interlaboratory study. *Anal. Chem.* **2012**, *84*, 7865−7873.

(21) Cumpson, P. J.; Portoles, J. F.; Sano, N. Material dependence of argon cluster ion sputter yield in polymers: Method and measurements of relative sputter yields for 19 polymers. *J. Vac. Sci. Technol., A* **2013**, *31*, 020605.

(22) Seah, M. P. Universal equation for argon gas cluster sputtering yields. *J. Phys. Chem. C* **2013**, *117*, 12622−12632.

(23) Seah, M. P. Argon cluster size-dependence of sputtering yields of polymers: Molecular weights and the universal equation. *Surf. Interface Anal.* **2015**, *47*, 169−172.

(24) Cumpson, P. J.; Portoles, J. F.; Sano, N.; Barlow, A. J. X-ray enhanced sputter rates in argon cluster ion sputter-depth profiling of polymers. *J. Vac. Sci. Technol. B* **2013**, *31*, 021208.

(25) Havelund, R.; Seah, M. P.; Shard, A. G.; Gilmore, I. S. Electron flood gun damage effects in 3d secondary ion mass spectrometry imaging of organics. *J. Am. Soc. Mass Spectrom.* **2014**, *25*, 1565−1571.

(26) Miyayama, T.; Sanada, N.; Bryan, S. R.; Hammond, J. S.; Suzuki, M. Removal of Ar⁺ beam-induced damaged layers from polyimide surfaces with argon gas cluster ion beams. *Surf. Interface Anal.* **2010**, *42*, 1453−1457.

(27) Shard, A. G. Detection limits in xps for more than 6000 binary systems using al Al and Mg Kα x-rays. *Surf. Interface Anal.* **2014**, *46*, 175−185.

(28) Renault, O.; Lavayssière, M.; Bailly, A.; Mariolle, D.; Barrett, N. Core level photoelectron spectromicroscopy with al Al Kα excitation at 500nm spatial resolution. *J. Electron Spectrosc. Relat. Phenom.* **2009**, *171*, 68−71.

(29) Senoner, M.; Wirth, T.; Unger, W.; Escher, M.; Weber, N.; Funnemann, D.; Kromker, B. Testing of lateral resolution in the nanometre range using the bam-l002-certified reference material: Application to tof-sims iv and nanoesca instruments. *J. Surf. Anal.* **2005**, *12*, 78.

(30) Jones, E. A.; Lockyer, N. P.; Kordys, J.; Vickerman, J. C. Suppression and enhancement of secondary ion formation due to the chemical environment in static-secondary ion mass spectrometry. *J. Am. Soc. Mass Spectrom.* **2007**, *18*, 1559−1567.

(31) Cooks, R. G.; Busch, K. L. Matrix effects, internal energies and ms/ms spectra of molecular-ions sputtered from surfaces. *Int. J. Mass Spectrom. Ion Phys.* **1983**, *53*, 111−124.

(32) Fujimoto, H.; Edura, T.; Miyayama, T.; Sanada, N.; Adachi, C. Accurate measurement of dopant concentration in organic light-emitting diodes by combining high-performance liquid chromatography and tof-sims. *J. Vac. Sci. Technol. B* **2014**, *32*, 030604.

(33) Karras, G.; Lockyer, N. P. Quantitative surface analysis of a binary drug mixture—suppression effects in the detection of sputtered ions and post-ionized neutrals. *J. Am. Soc. Mass Spectrom.* **2014**, *25*, 832−840.

(34) Kucher, A.; Jackson, L. M.; Lerach, J. O.; Bloom, A. N.; Popczun, N. J.; Wucher, A.; Winograd, N. Near infrared (nir) strong field ionization and imaging of C60 sputtered molecules: Overcoming matrix effects and improving sensitivity. *Anal. Chem.* **2014**, *86*, 8613−8620.

(35) Shard, A. G.; Rafati, A.; Ogaki, R.; Lee, J. L. S.; Hutton, S.; Mishra, G.; Davies, M. C.; Alexander, M. R. Organic depth profiling of a binary system: The compositional effect on secondary ion yield and a model for charge transfer during secondary ion emission. *J. Phys. Chem. B* **2009**, *113*, 11574−11582.

(36) Shard, A. G.; Spencer, S. J.; Smith, S. A.; Havelund, R.; Gilmore, I. S. The matrix effect in organic secondary ion mass spectrometry. *Int. J. Mass Spectrom.* **2015**, *377*, 599−609.

(37) Dollery, C. Intracellular drug concentrations. *Clin. Pharmacol. Ther.* **2013**, *93*, 263−266.

(38) Braggio, S.; Montanari, D.; Rossi, T.; Ratti, E. Drug efficiency: A new concept to guide lead optimization programs towards the selection of better clinical candidates. *Expert Opin. Drug Discovery* **2010**, *5*, 609−618.

(39) Wernecke, J.; Shard, A. G.; Krumrey, M. Traceable thickness determination of organic nanolayers by x-ray reflectometry. *Surf. Interface Anal.* **2014**, *46*, 911−914.

(40) Shard, A. G.; Spencer, S. J.; Smith, S. A.; Havelund, R.; Gilmore, I. S. The matrix effect in organic secondary ion mass spectrometry. *Int. J. Mass Spectrom.* **2015**, *377*, 599.

(41) Shard, A. G.; Havelund, R.; Spencer, S. J.; Smith, S. A. *Vamas twa 2, 2014: Sub-project a3(g) static sims interlaboratory study: Organic depth profiling of mixed materials—protocol for analysis*; 2014.